AIAA JOURNAL
Vol. 43, No. 4, April 2005

Unsteady Calibration of Fast-Response Pressure Probes, Part 2: Water-Tunnel Experiments

Espen S. Johansen* and Othon K. Rediniotis†
Texas A&M University, College Station, Texas 77843-3141

This part of our work presents the development of a water-tunnel setup to experimentally determine the instantaneous pressure distribution over a sphere in unsteady flow, the unsteady pressure coefficient, and to provide validation of the unsteady probe calibration techniques discussed in Part 1 (Johansen, E. S., and Rediniotis, O. K., "Unsteady Calibration of Fast-Response Pressure Probes, Part 1: Theoretical Studies," *AIAA Journal*, Vol. 43, No. 4, 2005, pp. 816–826). To generate an unsteady flowfield with significant inertial effects, a water-tunnel setup was developed where flow unsteadiness was generated by oscillating a spherical probe with a diameter of 50.8 mm at frequencies up to 4 Hz. The steady and unsteady pressure coefficients were experimentally determined, and it was found that both compared well with unsteady potential flow theory. These coefficients were subsequently used to test the unsteady probe calibration algorithms at different oscillation frequencies and flow angles. Good flow prediction capabilities were demonstrated. The importance of this work mainly lies in the fact that it provides experimental determination of the unsteady pressure coefficient and validation of the unsteady multihole probe calibration technique developed in Part 1.

Nomenclature

Cp	=	pressure coefficient
Cp_S	=	steady pressure coefficient
Cp_{STEADY}	=	steady pressure coefficient
Cp_U	=	unsteady pressure coefficient
Cp_{UNSTEADY}	=	unsteady pressure coefficient
K	=	nondimensional acceleration
p	=	pressure, Pa
p_s	=	static pressure, Pa
p_t	=	total pressure, Pa
q_{dyn}	=	dynamic pressure, Pa
R	=	probe tip radius, m
$U(t)$	=	instantaneous velocity, m/s
$\bar{U}$	=	mean velocity, m/s
θ	=	cone angle and coordinate measuring from the stagnation point, deg
ρ	=	density, kg/m^3

Introduction and Background

AERODYNAMIC multihole probes can measure flow angle and flow velocity from the pressure distribution over the probe tip (measured at discrete ports). The pressure distribution over the tip in steady flowfields is a function of velocity magnitude (dynamic head), flow angle, and tip geometry. In addition to these, the pressure distribution over the tip of a probe in unsteady flowfields depends on the rate of change, or acceleration, of the flowfield. Using a conventional probe calibration algorithm without properly accounting for the unsteady flow effects can yield large errors. A validated unsteady calibration technique is therefore necessary before fast-response multihole probes can be used for accurate measurements in unsteady flowfields. The algorithm developed in Part 1 requires that the both the steady and unsteady pressure coefficients are known.

Received 6 June 2002; accepted for publication 7 July 2004.

*Postdoctoral Research Associate, Department of Aerospace Engineering. Member AIAA.
†Associate Professor, Department of Aerospace Engineering. Associate Fellow AIAA.

If the flow over the tip of a hemispherical probe is modeled as the flow over the front (windward) side of a sphere, then the instantaneous pressure coefficient on the tip is given in terms of a steady and an unsteady component [see also Part 1 (Ref. 1)]:

$$\frac{p(\theta,t)-p_S}{1/2\rho U^2} = Cp(\theta,t) \equiv Cp_{\text{STEADY}} + Cp_{\text{UNSTEADY}} \tag{1}$$

where

$$Cp_{\text{STEADY}} = \left[\tfrac{9}{4}\cos^2(\theta) - \tfrac{5}{4}\right] \tag{2}$$

$$Cp_{\text{UNSTEADY}} = \frac{R}{U(t)^2}\frac{\mathrm{d}U(t)}{\mathrm{d}t}\cos(\theta) = K(t)\cos(\theta) \tag{3}$$

or

$$Cp(\theta,t) = Cp_S(\theta) + K(t)Cp_U(\theta) \tag{4}$$

where

$$Cp_{\text{STEADY}} = Cp_S, \qquad Cp_{\text{UNSTEADY}} = K(t)Cp_U$$
$$Cp_U = \cos(\theta) \tag{5}$$

The experimental determination of the unsteady pressure coefficient Cp_U is as crucial as it is challenging and has seen significant disagreement in the literature. The need for experimental determination and validation of the unsteady pressure coefficient arises from the fact that the preceding theory assumes a perfect sphere and not an imperfect hemisphere, which represents a typical probe tip. Moreover, the preceding theory ignores viscous effects. The existing literature shows significant controversy in the experimental determination of the unsteady pressure coefficient. The study undertaken by Kovasznay et al.[2] made several assumptions in the theoretical model of the inertial effects: the amplitude of oscillation must be small, and the ratio of the flow unsteadiness wavelength to the probe diameter must be large. Additionally, they used a condenser microphone to measure the surface pressure on the sphere. This microphone was placed 20 mm away from the measurement point on the sphere surface and was connected to it via tubing. In addition, there was a significant cavity volume in front of the transducer diaphragm. Although a prediction was made on the transfer function of this tubing-cavity-transducer system, the pressure attenuation was corrected by matching the measured pressures to those predicted by their theoretical model for the inertial effects on the

sphere. The phase lag was also corrected in a similar manner. Therefore, their theoretical model on the inertial effects was not validated by their experimental data. The theoretical potential flow model, for a sphere, predicts a Cp_U coefficient of 1.0 at the stagnation point. Their work found that this coefficient for a sphere should be 3.0 at the forward stagnation point. This discrepancy is too large to be a result of viscous effects or deviations of the actual geometry from a perfect sphere. This discrepancy prompted us to further analysis to accurately determine the pressure distribution over the hemispheres in unsteady flowfields.

Cylinders, spheres, and ellipses in unsteady flowfields have been analyzed computationally by a number of researchers.[3–8] However, the emphasis of these studies has mainly been on oscillating flows with zero mean, and integral quantities such as drag were reported rather than pressure distributions.

Humm and Verdegaal[9] designed a system for experimental determination of the unsteady flow effects on a number of different probe geometries. For their tests, the probes were oscillated using a system comprised of a dc-motor driving a crankshaft and pushrod connected to a linear slide. This assembly was towed in a 40-m stationary water channel, yielding a probe relative velocity equal to the sinusoidal oscillation velocity superimposed on the towing velocity. Scaled-up (30-mm) cylinder and wedge-shaped probes were used to match the Reynolds number and nondimensional frequency ranges typically encountered in turbomachinery applications. Significant inertial effects were identified for the longitudinal oscillations. Based on the work by Kovasznay et al.,[2] Humm and Verdegaal[9] postulated a method to correct the dynamic effects based on the acceleration of the fluid. The same facility could also be used to generate sinusoidal oscillations in yaw angle. Large dynamic circulation effects were identified for wedge-shaped probes, whereas for cylindrical- or half-cylinder-shaped probes these effects were much less pronounced.

Following the work by Kovasznay et al.[2] and Humm and Verdegaal,[9] a similar effort was undertaken to experimentally determine the unsteady pressure distribution over an oscillating sphere in water. It was shown in Part 1 (Ref. 1) that the unsteady or inertial effects increase with increasing magnitude of the nondimensional rate of unsteadiness K. To experimentally determine the unsteady pressure coefficient, it is preferred to have a magnitude of K as large as possible to ensure significant and distinguishable inertial effects. From the definition of the nondimensional acceleration $\{K = [R/U(t)^2][\mathrm{d}U(t)/\mathrm{d}t]\}$, this can be obtained in three different ways: large probe size, high unsteadiness frequency, or low velocity. For air tests, very low velocity will result in low signal to noise because of the low sensitivity of the pressure transducer (most miniature or micropressure transducers have ranges on the order of psi). As discussed in Part 3 (Ref. 10), with respect to the unsteady calibration in air, the need to have a repeatable, periodic, well-behaved, fluctuating airstream has limited us to oscillation frequencies below 1000 Hz. This, combined with the diameter of the probe that can be used in the air facility ($\frac{1}{4}$ in.; 6.35 mm), has limited the inertial effects to less than 5% [see Part 3 (Ref. 10)]. To generate inertial effects of significantly higher magnitude and thus be able to accurately determine the unsteady pressure coefficient as well as achieve verification of our unsteady probe calibration methods, we have developed a water-tunnel unsteady flow setup. In water, the much higher density provides significant dynamic pressures at low velocities. Also, by using a large probe the frequency of the flow unsteadiness can be kept low while still matching the Reynolds number range and K values that would be seen for a miniature probe in air.

Measurement of the instantaneous dynamic pressure in water is challenging because most commercially available miniature pressure transducers, with the required sensitivity, are designed for nonconductive gases. Ciocan et al.[11] used a five-hole fast-response cobra probe with a 7-mm-diam pyramidal tip to measure the unsteady flow at the exit of a hydraulic pump. The probe had seven miniature fast-response pressure transducers mounted in the tip, and the dynamic response was tested using an electric spark in a water tank. The sparks created a vapor bubble that generated a shock wave in the tank when imploded. It was found that the transducers were highly photosensitive, which contaminated the dynamic response. The photosensitivity also impeded the simultaneous use of an laser-Doppler-velocimetry system. Ciocan et al.[11] also reported difficulties with large drift of the transducer output.

For our facility, the flow velocity relative to the probe is derived by the motion of the probe superimposed on the steady water-tunnel velocity. This flowfield possesses slightly different properties than unsteady flowfield over a stationary probe; the stagnation pressure throughout the flowfield is constant at each instant of time. However, similar to Kovasznay et al.,[2] it is assumed that the wavelength of the unsteadiness is significantly longer than the probe diameter.

Experimental Setup

A system consisting of a crankshaft and a pushrod mounted to an electric motor was constructed to oscillate the probe in a sinusoidal manner. Figures 1 and 2 show the conceptual design of the system. The crankshaft is mounted on the dc motor and a flywheel, connecting the pushrod to a linear motion system that allows linear translation only. The instantaneous position of the probe was measured using a linear variable differential transformer (LVDT) with an output voltage linearly proportional to the position of the sliding assembly. The probe velocity is calculated as the derivative of the position given by the LVDT.

Figure 2 shows the schematic of the probe assembly mounted in the water tunnel. The vertical probe mount is connected to the linear motion system with eight rubber vibration dampers. It was found that without these dampers high-frequency structural vibration was transmitted from the linear bearing to the probe shaft, and a significant ~250-Hz signal was observed in the measured probe pressure. The vibration dampers cause some loss of rigidity in the vertical mount. The displacement of the end of the vertical bar was measured for a range of loads (simulating the loads from the acceleration). Negligible deflection (<1 mm) was observed for the range of loads corresponding to the range of testing frequencies (2–4 Hz). The entire probe assembly is mounted in a clamp and can be manually rotated (about a vertical axis that goes through the probe tip) to any angle while the probe tip remains stationary (Fig. 3). Although the assembly allows for full 360-deg rotation, the range of interest is limited to 0–90 deg from the freestream direction. Herein, this angle will be referred to as the probe cone angle θ.

A 50.8-mm-diam spherical probe (Figs. 3 and 4) with a pressure port located at the forward center point was designed to house a

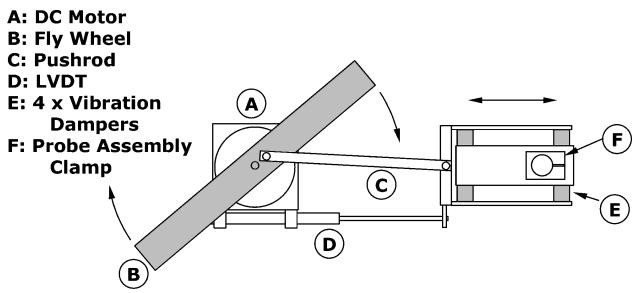

Fig. 1 Schematic of the crankshaft linear motion system.

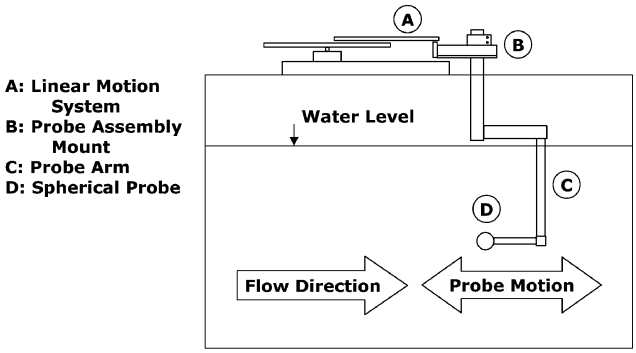

Fig. 2 Schematic of the water-tunnel setup.

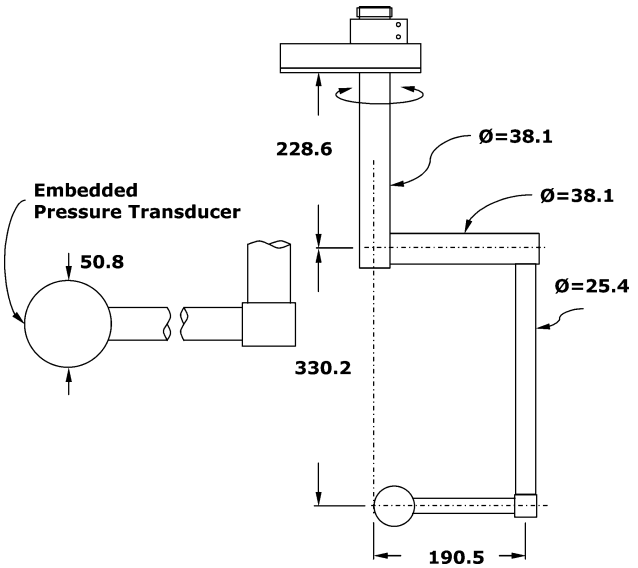

Fig. 3 Probe mounting assembly (dimensions in millimeters). The probe can be rotated by 360 deg.

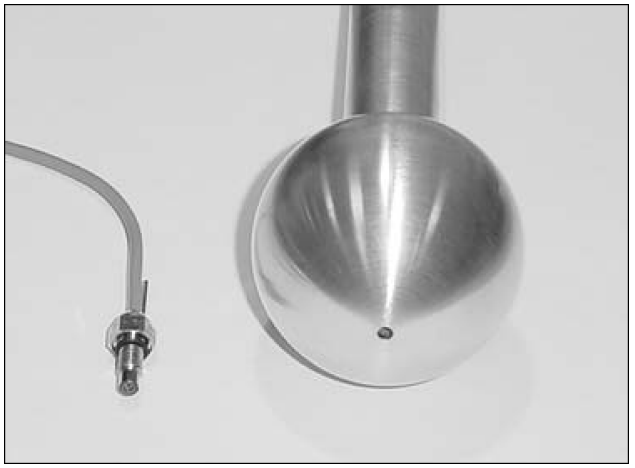

Fig. 4 Modified COTS pressure transducer and the spherical probe head.

modified commercial-off-the-shelf (COTS) fast-response, high sensitivity (30 mV/kPa) transducer and a fixed-gain (100) amplifier. The transducer employs a four-arm piezoresistive bridge mounted on a sculptured silicon diaphragm and features an internal temperature compensation module. The COTS transducer was designed for dry gas, but was modified for water usage by the manufacturer. The protective screen in front of the diaphragm was removed and replaced with a nonconducting gel to ensure that the diaphragm is not directly exposed to water. Figure 4 shows pictures of the spherical probe and the transducer.

The pressure transducer was calibrated to a high-accuracy reference pressure transducer by placing the entire probe assembly in a pressure chamber (Fig. 5). The results are shown in Fig. 6, and excellent linearity and negligible drift are observed. However, because the transducer was used in water, the in-air calibration was also validated in water. The probe was mounted on a computer-controlled traverse, and the probe was submerged vertically into the water tunnel in 25.4-mm increments. At each position, the voltage was recorded and correlated to the hydrostatic pressure. The water calibration obtained in this way agreed well with the air calibration plotted in Fig. 6 and showed that the modified pressure transducer has equal sensitivity in air and water.

The acceleration of the probe and the transducer, as a result of the oscillatory motion, causes a false periodic signal to be imposed on the measured pressure. The unmodified version of the transducer has low acceleration sensitivity equivalent to 1.4 Pa/g. However,

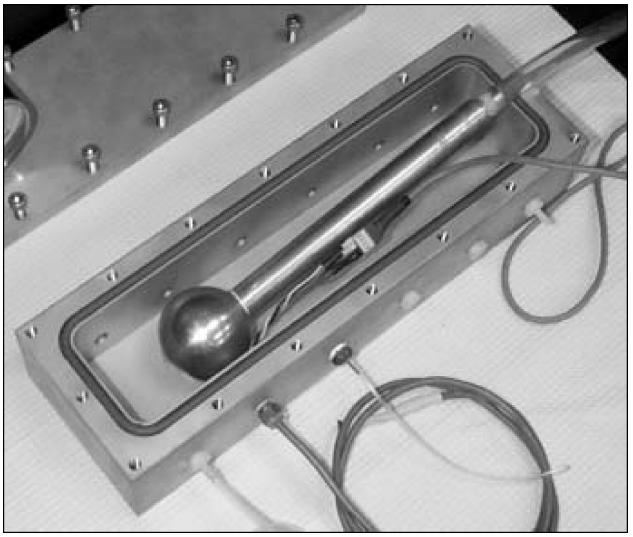

Fig. 5 Pressure transducer calibration chamber.

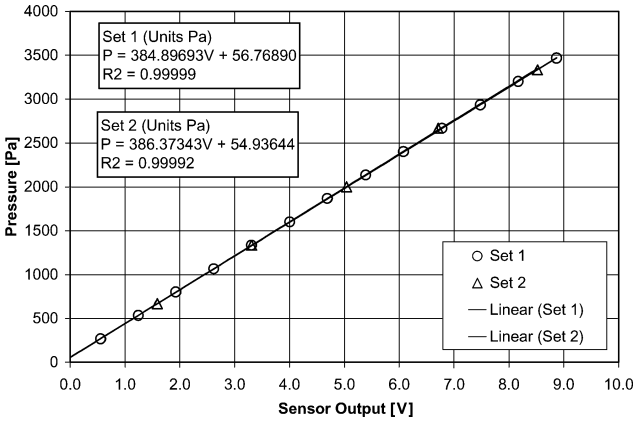

Fig. 6 Calibration of the modified COTS transducer in air, showing very good linearity and negligible zero drift for two data sets taken 1 h apart with 20-min warm-up time before first set.

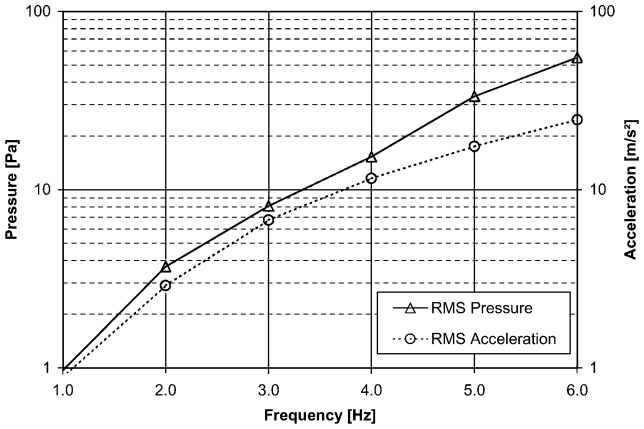

Fig. 7 Effects of axial acceleration on the pressure transducer.

because the modified version has the gel directly on the diaphragm a set of tests was performed to quantify the acceleration sensitivity. The probe was mounted on the linear motion system and oscillated at 1–6 Hz in air. The acceleration sensitivity was found to be approximately 12 Pa/g, based on the data shown in Fig. 7. All data sets were consequently corrected using the acceleration sensitivity multiplied with the cosine of the probe angle.

The experiments were conducted in a 2×3 ft water tunnel facility. The water tunnel is a free-surface, closed-circuit facility that holds approximately 20,000 liters of water and has a 0.6-m-wide, 1-m-deep, and 2-m-long test section. The tunnel is powered by a 25-Hp

pump, with flow rates up to 470 liters per second, yielding test section velocities up to 0.9 m/s. The tunnel has a 6:1 contraction ratio and <1% rms turbulence level, <2% velocity nonuniformity, and <1 deg flow angularity in both pitch and yaw.

The test-section velocity was measured by injecting dye into the stream approximately 0.3 m below the surface and measuring the time for the dye to travel between two marks placed 1.5 m apart. A modified stopwatch with two switches for start and stop was used in the following way: one person starts the stopwatch when the dye passes the first line, and the second person stops the timer when the dye passes the second line. Naturally, such measurements have errors as a result of the reaction time of the persons starting and stopping the clock and the diffusion of the dye. For the tests, 52 repeated samples were taken, to provide a statistical distribution of the measurement. As shown in Fig. 8, the mean measured time for one velocity setting was 1.74 s with a standard deviation of 0.081 s. Using a 95% confidence interval and a sample size of 52 (no samples were rejected as outliers), the velocity was determined to be 0.86 m/s $\pm$ 1.3%. The experiment was repeated with the two persons trading places, and this yielded virtually identical results. Although different means of velocity determination could also be used, such as our particle image velocimetry system, the marginally better accuracy did not warrant the additional complications.

The water tunnel has a free surface, and the water level in the test section drops with increasing flow rates. The decreased water column relative to the probe is seen as a decrease in average pressure. For each millimeter of water level decrease, the associated pressure is approximately 10 Pa lower; hence, the change in water level (up to 50 mm or 500 Pa) from zero velocity to running velocity must be accurately known, and the probe pressure must be corrected accordingly. In addition to the mean drop in water level in the test section, waves with an approximate magnitude of 5 mm peak to peak and wavelength on the order of meters were also observed. This periodic increase and decrease in water column above the probe also shows up in the measured pressure, and hence these waves must be accounted for. A static-pressure probe with an embedded pressure transducer was designed to measure the water column without measuring the stagnation pressure from water velocity. The probe in Fig. 9 has an embedded COTS pressure transducer with a range of 12 kPa. It was placed in the water tunnel with the pressure port at approximately the same depth as the spherical probe (Fig. 10). The exact depth was not crucial because differential quantities were sought. Figure 10 shows the water-tunnel setup, illustrating some of the main components.

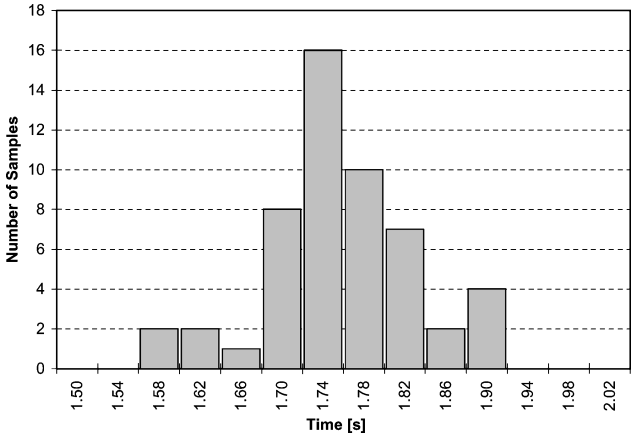

Fig. 8 Distribution of measured times for the water-tunnel freestream dye tests.

Data Analysis

Assuming constant rotation speed of the crankshaft, the experimental envelope is as shown in Table 1. Important parameters in Table 1 are the mean probe-relative velocity, providing insight into the Reynolds number and the mean dynamic pressure. The minimum probe-relative, instantaneous velocity must never go below zero to avoid flow reversal. The acceleration should also be below values corresponding to nonnegligible deflections of the probe mount. The nondimensional acceleration K is a measure of the inertial effects on the probe [Eq. (3); see also Part 1 (Ref. 1)]. As seen in the table, the maximum values of K are very large for frequencies above 3 Hz. This is because of the inverse proportionality to the square of the velocity and the fact that the probe relative velocity is very low during the downstream motion of the probe. The mean Reynolds number (based on probe diameter) for the probe at the test velocity is approximately 4×10^4, which is in the range seen by miniature multihole probes in airflows.

Time series of three basic quantities were sought: probe-sensed dynamic pressure, probe relative flow velocity, and probe relative flow acceleration. As just noted, the static-pressure probe and the spherical probe were both exposed to a significant pressure as a result of the water column above the sensors. However, these pressure readings were offset to give zero pressure readings for zero flow velocity. As the freestream velocity is increased from zero to the test velocity, the water level in the test section drops, and the static-pressure sensor records a negative pressure proportional to the decrease in water column. Similarly, the spherical probe records the drop in hydrostatic pressure, but in addition it also measures and increase in pressure as a result of the flow dynamic pressure. To find the true dynamic pressure sensed by the spherical probe, the static probe pressure was subtracted from the measured spherical probe pressure. For the entire time series, both the static and spherical

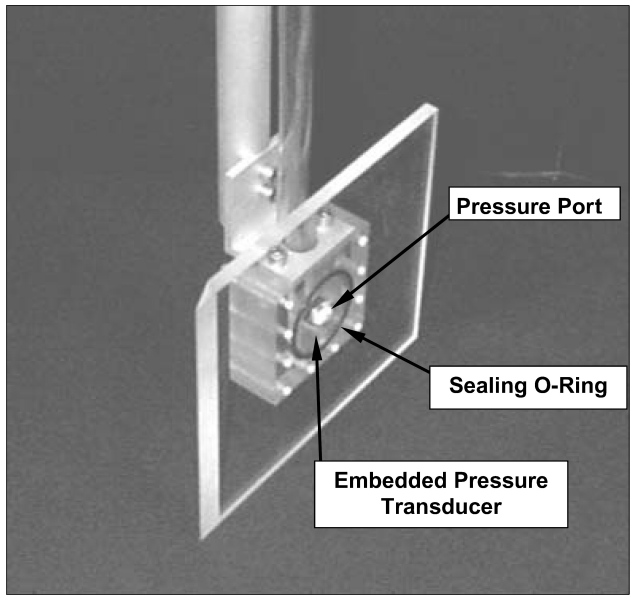

Fig. 9 Static-pressure probe.

Table 1 Test matrix for the spherical probe in the water tunnel

Frequency, Hz	Case	Mean velocity, m/s	Maximum relative velocity, m/s	Minimum relative velocity, m/s	Maximum acceleration, m/s^2	Maximum K
1	——	0.85	1.01	0.69	1.08	0.04
2	——	0.85	1.17	0.53	4.35	0.20
3	3	0.85	1.33	0.37	9.78	0.67
4	1,2	0.85	1.49	0.21	17.38	2.49

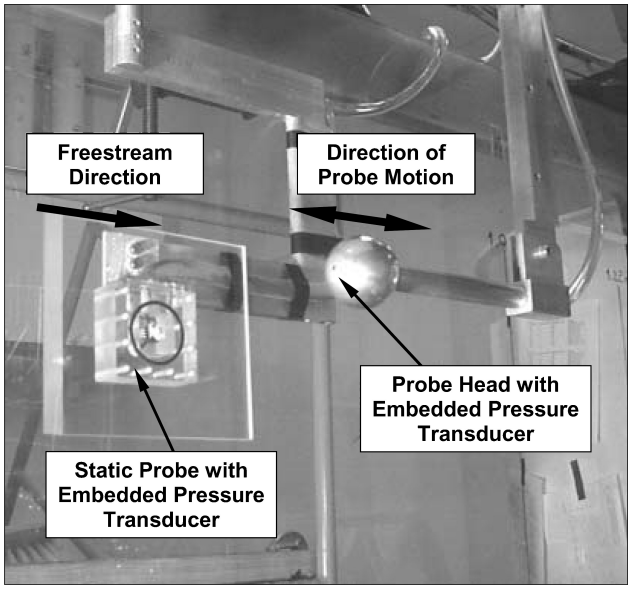

Fig. 10 Static probe and spherical probe mounted in water-tunnel facility.

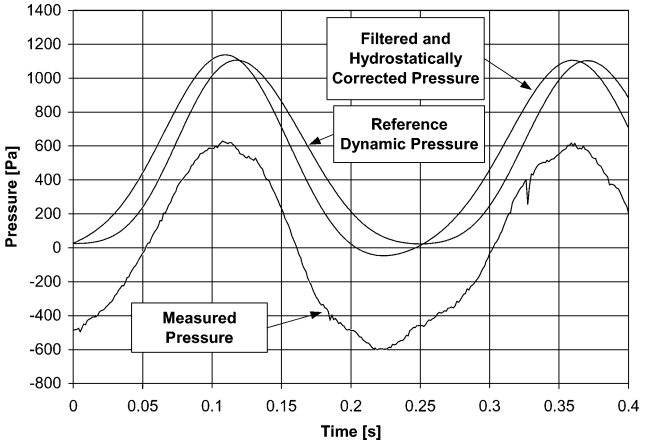

Fig. 11 Data for a frequency of 4 Hz, tunnel velocity of 0.85 m/s, and 0-deg cone angle (test case 1).

probe pressures were sampled simultaneously, and the hydrostatic correction was performed on a point-by-point basis (on filtered data).

The probe oscillation is nearly sinusoidal for a constant rotation speed of the crankshaft. However, no assumptions are made regarding the motion, and the LVDT is sampled concurrently with the pressure signal. The position sensor was calibrated for the range of translation, with the maximum and minimum values given by the radius of the crankshaft. As with all digitized data, the present data time series are not perfectly smooth for two reasons: the resolution of the DAQ system (2.44 mV) and noise floor (on the order of 10 mV p-p). From the discretely digitized data, the derivatives could not be calculated without low-pass filtering the data. A conventional finite impulse response filter with a large sample size (2^{14} data points) was used with all sampled data. The sampling frequency was adjusted to 200 times the oscillation frequency, yielding 200 points per period and more than 80 periods of oscillation in each data set. Measured, filtered, and hydrostatically corrected quantities are shown in Fig. 11 for a frequency of 4 Hz and zero cone angle.

Measurement of Steady and Unsteady Pressure Coefficients

We will call "true dynamic pressure" the dynamic pressure corresponding to the instantaneous probe relative velocity ($q_{\text{dyn}} = \frac{1}{2}\rho U^2$). This is the pressure the probe would measure (relative to static), at

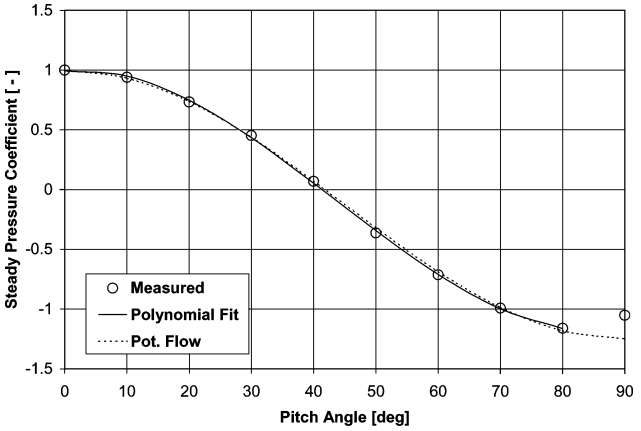

Fig. 12 Steady pressure coefficient calculated from the experimental spherical probe data. The data are curve fitted and plotted up to 90 deg. The Reynolds number is subcritical, and laminar separation is observed.

zero cone angle, in the absence of inertial effects. However, the measured pressure at the forward stagnation point has larger magnitude and leads the true dynamic pressure in phase caused by the inertial effects. This is clearly seen in the two top curves in Fig. 11. The fact that the measured dynamic pressure should lead and be larger than the true dynamic pressure follows from the theory established in Part 1 (Ref. 1). Moreover, the former and the latter should be the same at points of zero flow acceleration. As seen in Fig. 11, the experimental data clearly illustrate and validate both of these theoretical predictions.

Steady Pressure Coefficient

The steady pressure coefficient was calculated from the pressures measured by the probe in steady flow (probe not oscillated) for cone angles ranging from 0 to 90 deg (Fig. 12). The experimentally determined steady pressure coefficient is seen to follow the potential flow theoretical predictions very well except for the last point at 90 deg, where the flow has separated. The significance of the good agreement seen in Fig. 12 is twofold: it shows the applicability of potential flow theory to our problem and the almost negligible effects of viscosity, while it validates our data acquisition and correction procedures.

Unsteady Pressure Coefficient

Determination of the unsteady pressure coefficient is significantly more challenging. The theoretical values are given from potential flow to follow $\cos(\theta)$ for axisymmetric flow over a sphere. To validate this prediction, the following procedure is followed. Equations (1–3) are combined and solved for the unsteady pressure coefficient, in terms of the measured port pressure. Note that Eqs. (6) and (7) show Cp_U as a function of time; however, this is done on purpose to indicate that Cp_U must be evaluated from data corresponding to the same point in time. Cp_U is only a function of cone angle:

$$Cp_U(\theta, t) = \frac{[p(\theta, t) - p_S] - \frac{1}{2}\rho U(t)^2 Cp_S(\theta)}{\frac{1}{2}\rho R[\mathrm{d}U(t)/\mathrm{d}t]} \tag{6}$$

or equivalently

$$Cp_U(\theta, t) = \left\{ \frac{[p(\theta, t) - p_S]}{\frac{1}{2}\rho U(t)^2} - Cp_S(\theta) \right\} \Big/ K(t) \tag{7}$$

As seen from Eq. (7), for an accurate determination of the unsteady coefficient it is necessary to choose data from a time series where the inertial effects are significant (as large nondimensional acceleration K as possible to avoid close-to-zero denominator values). For each point in the time series, the value of K was calculated, and only data points that were above an absolute value of $K = 0.2$ were used to find an average unsteady pressure coefficient for that

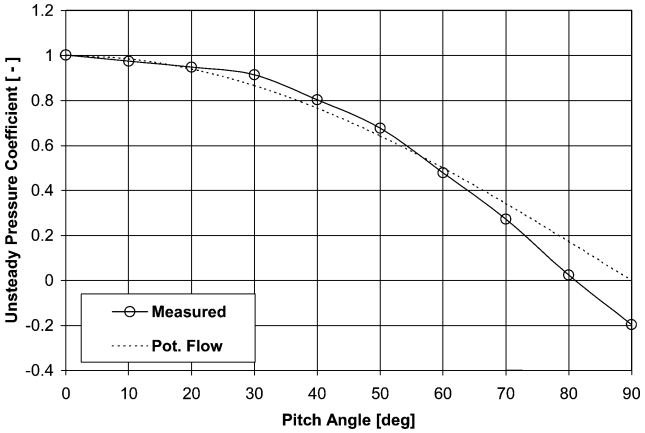

Fig. 13 Calculated unsteady pressure coefficient from experimental data at f = 4 Hz.

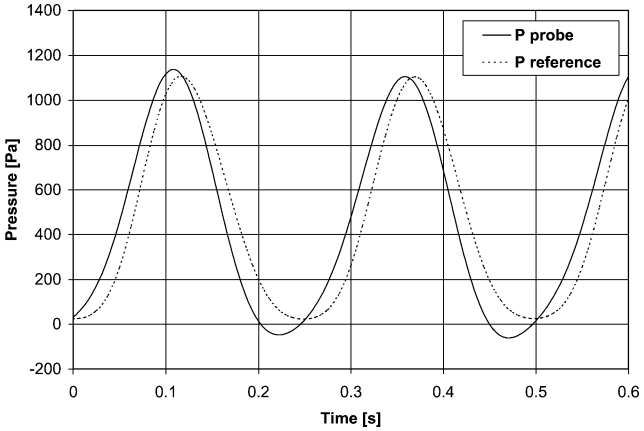

Fig. 14 Filtered sphere pressure and the true probe relative dynamic pressure of the flow for f = 4 Hz and cone angle of 0 deg (case 1).

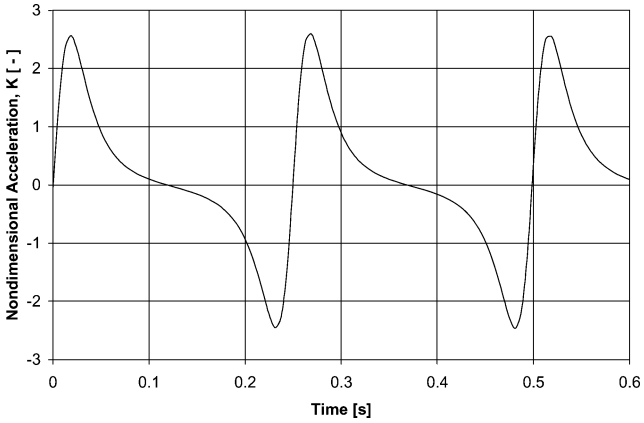

Fig. 15 Nondimensional acceleration K for f = 4 Hz and cone angle of 0 deg (case 1).

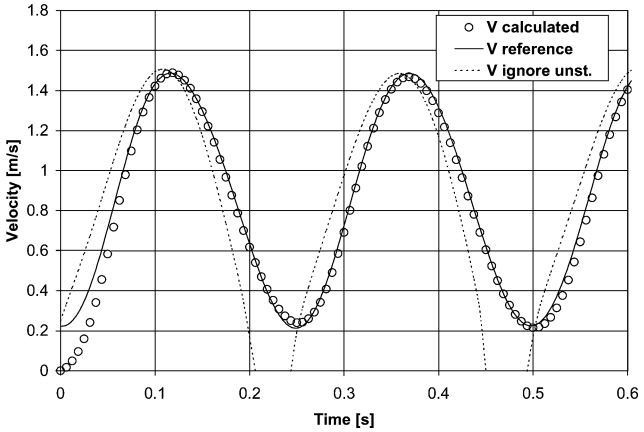

Fig. 16 Velocity prediction using the numerical routine for f = 4 Hz and cone angle of 0 deg (case 1).

angle. The results are shown in Fig. 13. The agreement between the experimentally determined unsteady pressure coefficient and that determined by unsteady potential flow theory is remarkable, especially for angles below 60 deg.

The standard deviation in the predicted mean value for the unsteady coefficient was large; however, the large number of points used to predict the mean unsteady Cp gave a 95% confidence interval for the mean value to ± 0.015 up to 30 deg, but increasing up to ± 0.03 for higher angles. The largest error source is believed to be the probe velocity calculated by differentiation of the filtered position sensor. Relative probe velocity could alternatively be achieved with, for example, a calibrated hot-film probe mounted to the linear motion assembly in parallel with the spherical probe.

The main purpose of the water-tunnel tests was to experimentally determine the steady and unsteady pressure coefficients as well as validate the theory and procedures for unsteady probe calibration, derived in Part 1 (Ref. 1). The spherical probe used in this analysis has only one pressure sensor and predicting, from a single pressure measurement, simultaneously the instantaneous velocity and flow angle is impossible. For this reason, the flow incidence angle (cone angle) was set at constant and known values, and determination of the velocity magnitude followed the procedures outlined in Part 1 (Ref. 1). The experimentally determined steady and unsteady pressure coefficients calculated in this part were used to predict the velocity magnitude for several time series of the spherical probe pressures. From the filtered data, the "exact" relative velocity is known and is used as a reference for comparison.

Validation of Unsteady Probe Calibration Algorithms

Case 1: Frequency 4 Hz and Cone Angle 0 Deg

The first test case is for an oscillation frequency of 4 Hz. The inertial effects for this test are large, with a maximum nondimensional acceleration K of about 2.5. The filtered probe pressure and the reference dynamic pressure (calculated from the water velocity and the spherical probe motion) are shown in Fig. 14. Figure 15 shows the nondimensional acceleration calculated from the reference velocity and probe diameter. The data in Fig. 16 show that the velocity magnitude is predicted from the measured pressure with very good accuracy in both phase and amplitude. The dashed line represents the velocity magnitude that would have been calculated if the inertial effects were ignored. As seen there, the errors made are very large (expected because of the large maximum value of K), especially close to the troughs of the waveform. In the trough, the measured dynamic pressure is negative (pressure lower than static pressure), and direct calculation of velocity is not possible.

The error of the Runge–Kutta-based numerical velocity calculation procedure is proportional to the step size to the fourth power (error $\propto h^4$); thus, for each doubling of the sampling frequency (halving the time between data) the error is expected to be reduced by a factor of 16. In Part 1 (Ref. 1), it was shown that with only 20 points per period very good predictions could be achieved. The data in the water-tunnel tests were sampled with 200 points per period, and thus very small errors are expected from the numerical routine.

Case 2: Frequency 4 Hz and Cone Angle 20 Deg

The oscillation frequency is 4 Hz yielding a maximum nondimensional acceleration K of 2.5. The unsteady CP corresponding to 20-deg incidence angle is 0.95 (potential flow 0.94) reducing the inertial pressure contribution by approximately 5% from the zero-angle case. In addition, for nonzero cone angle the measured pressure has significantly shifted phase from the reference dynamic pressure. In this test, the cone angle is known, and the steady and

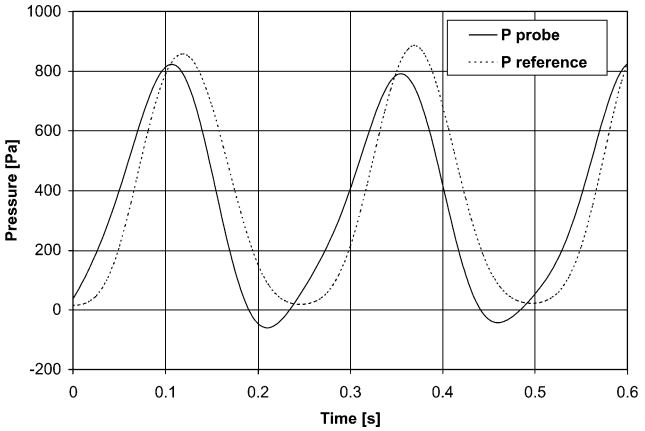

Fig. 17 Filtered sphere pressure and true probe relative dynamic pressure of the flow for f = 4 Hz, and cone angle of 20 deg (case 2).

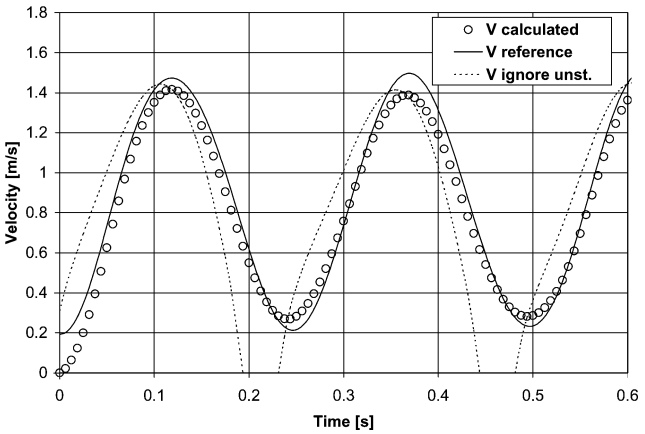

Fig. 18 Velocity prediction using the numerical routine for f = 4 Hz and cone angle of 20 deg (case 2).

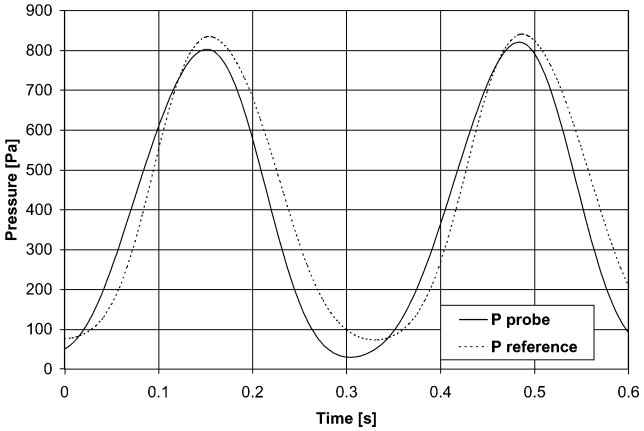

Fig. 19 Filtered sphere pressure and true probe relative dynamic pressure of the flow for f = 3 Hz and cone angle of 10 deg (case 3).

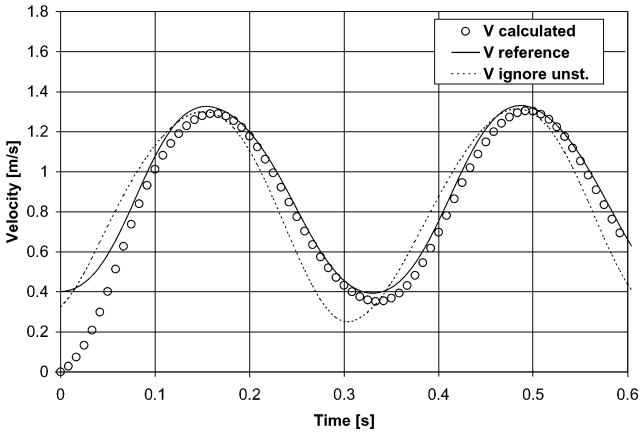

Fig. 20 Velocity prediction using numerical routine for f = 3 Hz and cone angle of 10 deg (case 3).

unsteady pressure coefficient values are given directly by the curve-fitted data from Figs. 12 and 13. Figure 17 shows the filtered spherical probe pressure and the true dynamic pressure of the flow for a cone angle of 20 deg, illustrating the large amplitude and phase difference between the two. Using the numerical velocity calculation routine, the velocity is still predicted well, as shown in Fig. 18.

Case 3: Frequency 3 Hz and Flow Angle 10 Deg

For a frequency of 3 Hz, the inertial effects are smaller than for 4 Hz; however, the contribution is still significant and will result in a maximum error in dynamic pressure of up to 67% if ignored (Table 1). The experimental determination of the unsteady pressure coefficient was based on data recorded at 4 Hz; hence, using the unsteady pressure coefficient to determine the velocity magnitude at 3 Hz, will show the technique's independence from frequency. In Fig. 19, large inertial effects are still seen for this lower frequency (as compared to 4 Hz). Figure 20 shows that for frequencies different from the calibration frequency the method works well in predicting the velocity magnitude.

As was just discussed, the indirect method of measuring the probe relative velocity can introduce nonnegligible errors, which means that in the three examples just given the error might not be in the predicted velocity, but rather the exact or reference velocity. Additional refinement could also be achieved in the starting points for the velocity calculation routine. Because of the nonlinearity of the governing equation, instability problems can occur in the starting region unless proper numerical stability precautions are taken. For periodic flows this might not impose a problem because a long time series can be used and the first few periods can be discarded. However, for nonperiodic flows further refinement of the starting conditions might be required.

Conclusions

Fast-response pressure probes (single and multihole) are increasingly being applied to measurement of unsteady flowfields ranging from separated flow behind bluff bodies to interstage measurements in turbomachinery. Caution must be exercised, however, because unsteady flows affect the measured pressures and can result in significant errors if not properly accounted for. In developing and validating an unsteady pressure probe calibration technique, an accurate unsteady pressure coefficient Cp_U is required. There is significant disagreement in literature on the theoretical derivation and value of the unsteady pressure coefficient and the effect of probe geometry and viscosity.

Accurate experimental determination of the unsteady pressure coefficient requires a repeatable unsteady flowfield and a probe that is subject to large inertial effects. The nondimensional acceleration K describing the magnitude of the unsteady effects, is proportional to the rate of change of velocity and inversely proportional to the square of the flow velocity. The high density of water provides significant dynamic pressures even at low velocities. Moreover, in water the frequency of the flow unsteadiness can be kept low while still matching the Reynolds number range and K values that would be seen for a small multihole probe in unsteady airflow.

A water-tunnel system for unsteady calibration of a scaled-up spherical probe was developed, and experimental determination of the unsteady pressure coefficient was undertaken. A 50.8-mm-diam spherical probe was equipped with a fast-response pressure transducer and mounted on an oscillating linear traverse system. The assembly was placed in a water-tunnel facility with mean flow velocity up to 0.9 m/s. The traversing system could oscillate the probe with frequencies of up to 4 Hz and peak-to-peak displacement of 50.8 mm. These values, combined with the low freestream

velocities, yielded K values as high as 2.5. The instantaneous spherical probe pressures and the true dynamic pressure were recorded, and the steady and unsteady pressure coefficients were calculated. For a cone angle of 0 to 80 deg, the steady pressure coefficient was shown to follow potential flow very well (laminar separation observed beyond 80 deg). The unsteady pressure coefficient also followed the potential flow theory quite well, and the disagreement is attributed primarily to measurement uncertainties.

The steady and unsteady pressure coefficients were subsequently used to test our unsteady probe calibration algorithms at different flow unsteadiness frequencies and flow angles. Good agreement was seen between the corrected and reference measurements, verifying both the underlying theoretical model (potential flow) and the velocity correction routine.

Acknowledgments

This work was sponsored by the Air Force Office of Scientific Research under Grant/Contract F49620-98-1-0162. The authors thank Thomas Beutner, the Technical Monitor of the project, as well as his predecessor, Mark Glauser. The work was also supported by Aeroprobe Corporation under Project 32500-7260M. The authors also thank Rick Allen for building the probes and support hardware and Lance Traub for guidance in the initial stages in this work.

References

[1]Johansen, E. S., and Rediniotis, O. K., "Unsteady Calibration of Fast-Response Pressure Probes, Part 1: Theoretical Studies," *AIAA Journal*, Vol. 43, No. 4, 2005, pp. 816–826.

[2]Kovasznay, L. S. G., Tani, I., Kawamura, M., and Fujita, H., "Instantaneous Pressure Distribution Around a Sphere in Unsteady Flow," Office of Naval Research, Rept. N00014-67-0163-002, Washington, DC, Dec. 1971.

[3]Badr, H. M., "Oscillating Inviscid Flow over Elliptic Cylinders with Flat Plates and Circular Cylinders as Special Cases," *Ocean Engineering*, Vol. 21, No. 1, 1994, pp. 105–113.

[4]Badr, H. M., Dennis, S. C. R., and Kocabiyik, S., "The Initial Oscillatory Flow past a Circular Cylinder," *Journal of Engineering Mathematics*, Vol. 29, No. 3, 1995, pp. 255–269.

[5]Zhang, H., and Zhang, X., "Flow Structure Analysis Around an Oscillating Circular Cylinder at Low KC Number: A Numerical Study," *Computer and Fluids*, Vol. 26, No. 1, 1995, pp. 83–106.

[6]Alassar, R. S., and Badr, H. M., "Oscillating Viscous Flow over a Sphere," *Computer and Fluids*, Vol. 26, No. 7, 1997, pp. 661–682.

[7]Badr, H. M., and Kocabiyik, S., "Symmetrically Oscillating Viscous Flow over an Elliptic Cylinder," *Journal of Fluids and Structures*, Vol. 11, No. 7, 1997, pp. 745–766.

[8]Sarpkaya, T., de Angelis, M., and Hanson, C., "Oscillating Turbulent Flow with or Without a Current About a Circular Cylinder," *Journal of Offshore Mechanics and Arctic Engineering*, Vol. 119, May 1997, pp. 73–78.

[9]Humm, H. J., and Verdegaal, J. I., "Aerodynamic Design Criteria for Fast-Response Probes," *Proceedings of the 11th Bi-Annual Symposium on Measuring Techniques in Transonic and Supersonic Flows in Cascades and Turbomachines*, Hochschule der Bundeswehr, Munich, 1992.

[10]Johansen, E. S., and Rediniotis, O. K., "Unsteady Calibration of Fast-Response Pressure Probes, Part 3: Air Jet Experiments," *AIAA Journal*, Vol. 43, No. 4, 2005, pp. 835–845.

[11]Ciocan, G. D., Vonnez, F., Baudoin, J., and Kueny, J., "Unsteady Five-Sensor Probe Development for Hydraulic Machinery," *Proceedings of ASME Fluids Engineering Summer Meeting*, FEDSM98-5082, 1998, pp. 1–6.

R. Lucht
Associate Editor